Journal of Applied Polymer Science

Porous Palygorskite-Polythiophene Conductive Composites for Acrylic Coatings

Shixiang Zuo,[1,2] Chao Yao,[1,2] Wenjie Liu,[2] Xiazhang Li,[2] Yong Kong,[2] Xiaoheng Liu,[1] Huihui Mao,[2] Yingruo Li[3]

[1]School of Chemical Engineering, Nanjing University of Science and Technology, Nanjing 210094, People's Republic of China
[2]School of Petrochemical Engineering, Changzhou University, Changzhou 213164, People's Republic of China
[3]College of Chemistry, Beijing Normal University, Beijing 100875, People's Republic of China
Correspondence to: C. Yao (E-mail: yaochao420@163.com) or X. Liu (E-mail: xhliu@mail.njust.edu.cn)

ABSTRACT: Modified palygorskite-polythiophene (MPA-PTh) composites were prepared by chemical oxidative polymerization of palygorskite (PA) nucleartor with thiophene (Th) after the surface modification with γ-(2,3-epoxypropoxy) propytrimethoxysilane (KH-560). The MPA-PTh composites were doped in iodine vapor to create the porous palygorskite-polythiophene (PMPA-PTh) conductive composites. Fourier transform infrared spectra (FTIR), X-ray photoelectron spectroscopy (XPS), X-ray diffraction (XRD), scanning electron microscopy (SEM), transmission electron microscopy (TEM), N_2 adsorption–desorption isotherms using the Brunauer–Emmett–Teller method (BET) and electrochemical impedance spectrum (EIS) techniques were applied to characterize the modified PA and the prepared composites. According to FTIR and XPS, the KH-560 was bound to the PA surface and the iodine ion (I_3^- and I_5^-) entered the PTh molecular chains. XRD, SEM, TEM, BET, and EIS analysis confirmed that the doping of iodine not only transform the core–shell MPA-PTh into the PMPA-PTh but also improve the electrical conductivity of composites. The PMPA-PTh composites were fabricated that yield a volume resistivity of $\sim 2.44 \times 10^2\ \Omega$ cm and a internal resistances of $\sim 100\ \Omega$, and their BET surface area, BJH (Barrett–Joiner–Halenda) average pore size and BJH cumulative pore volume were improved in comparison with those of the MPA-PTh composites. SEM images showed that the PMPA-PTh composites could form consecutive space network and the PMPA-PTh composites acrylic coating films had advisable conductivity. © 2013 Wiley Periodicals, Inc. J. Appl. Polym. Sci. 129: 2707–2715, 2013

KEYWORDS: palygorskite; polythiophene; conductivity; porosity; coatings

Received 16 October 2012; accepted 9 January 2013; published online 30 January 2013
DOI: 10.1002/app.38995

INTRODUCTION

Conductive polymers, such as polyaniline (PANI), polypyrrole (PPy), and polythiophene (PTh), are attracting increasing interests in many potential applications including supercapacitors,[1] anticorrosion,[2] rechargeable batteries,[3] conductive coatings,[4] and so forth. As an important member in the family of all conductive polymers, PTh, especially its hybrid composites, has been the investigative hotspot during the recent decades due to its controllable conductivity, high environmental stability, and other unique properties.[5] PTh/TiO_2,[6] PTh/SnO_2,[7] PTh/Al_2O_3,[8] for instance, have been extensively studied. More recently, Uygun et al.[9] introduced the preparation and electrical conductivity property of PTh/SiO_2 nanocomposites using three different surfactants, and the results showed that the highest conductivity obtained was 2.7×10^{-2} S cm^{-1} in the existence of poly(ethylene oxide) (20) sorbitan monolaurate (Tween-20). To date, the experimental research of palygorskite (PA)-PTh composites has not been covered yet.

Nature PA, also called attapulgite, is a hydrated magnesium-aluminium silicate clay mineral with clusters of fibers,[10] and it can be disaggregated into numerous chopstick-like single crystals with high aspect ratio after physicochemical treatments such as ultrasonic agitation, mechanical shearing and high pressure homogenization.[11] The diameter of a single crystal is just dozens of nanometer and the length may reach micron scale. Besides, the single crystal has good mechanical strength,[12] which makes PA widely used in the realm of polymers such as plastic,[13] rubber[14] and coating. As a special and cost-effective functional inorganic material, PA is certainly an excellent nuclear body in preparing core–shell composites like PA-PANI and PA-PPy composites.[15,16]

In this article, PA was first modified with γ-(2,3-epoxypropoxy) propytrimethoxysilane (KH-560), and thus the MPA-PTh composites with well covered core–shell morphology were prepared by chemical oxidative polymerization. Based on the procedure

Applied Polymer SCIENCE

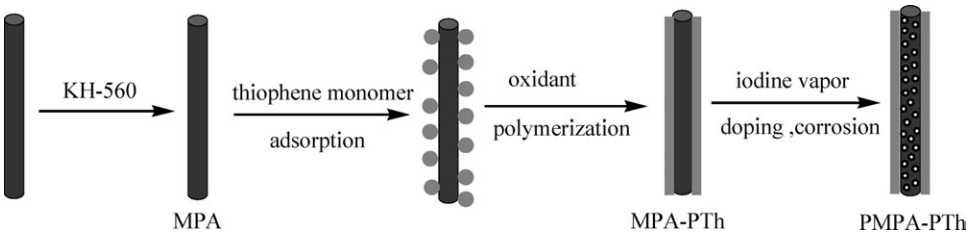

Scheme 1. The preparation of PMPA-PTh conductive composites.

that the MPA-PTh composites were doped in iodine vapor, we demonstrated that the MPA-PTh could be transformed into the porous MPA-PTh composites (PMPA-PTh). The process in preparation of the PMPA-PTh was shown as Scheme 1. Finally, the influences of the PMPA-PTh composites on the conductivity of acrylic coatings were investigated in detail.

EXPERIMENTAL

Materials and Reagents

PA (purity 99%) was supplied by Jiangsu NDZ Technology Group, KH-560 was provided by Nanjing Xinhuai Scientific, toluene, anhydrous ethanol, thiophene (Th), anhydrous ferric chloride ($FeCl_3$), iodine and acetone were purchased from Sinopharm Chemical Reagent, acrylic emulsion and other additives were purchased from Eternal Chemical, all chemicals were of analytical grade and deionized water was used throughout the experiments.

Preparation of Modified PA

The modified PA (MPA) was achieved by azeotropic distillation method. 2.0 g of acid-treated PA was dispersed in 40 mL of deionized water and 0.2 g of KH-560 was dissolved in 160 mL of toluene, respectively; and then they were mixed together in a 500 mL three-neck round-bottomed flask equipped with a stirrer, thermometer, and reflux condenser. The whole system was heated to azeotropy for several hours until the water was virtually droved out. The mixture was filtered out and washed with anhydrous ethanol to remove the surplus agent, and the filter cake was dried naturally at room temperature.

Preparation of PMPA-PTh

The obtained MPA was dispersed in 100 mL of toluene with stirring and ultrasonic agitation; subsequently, 1.60 g (0.019 mol) of Th monomer was added into the above dispersion. After stirring for 30 min at 10°C, 9.25 g (0.057 mol) of $FeCl_3$ in 200 mL of toluene solution was added dropwise within 30 min to start chemical oxidative polymerization of the monomer and the mixture was allowed to polymerize for another 12 h. Brown suspension was filtered out and washed with anhydrous ethanol to get wine red MPA-PTh composites, and then the MPA-PTh composites were dried in air at 60°C. Finally, the prepared MPA-PTh composites and iodine (0.4 : 1.0 mass ratio, iodine/composites) were put into a closed container at 120°C for 4 h. After this, the dark composites were achieved and washed several times with acetone. Immediately, the PMPA-PTh conductive composites were developed. For comparison, the pure PTh was also synthesized and doped under the same technological conditions. Meanwhile, PA-PANI and PA-PPy composites were prepared from our previous research.[17]

Preparation of Conductive Coating Films

The PMPA-PTh composites were dispersed into 100 g acrylic emulsion (AC-261) containing 50% solid content with ultrasonic vibrations, subsequently the system pH value was adjusted to 6–7 using $NH_3 \cdot H_2O$. 1.5 g defoamer (K-520), 4.0 g film forming auxiliary (DE-12) and 12.0 g thickener (KM-60) were added dropwise into the system with slight stirring. All the above mixture was also grinded at 4300 rpm for 30 min on DMQ-07 ball mill machinery (Qingdao Union Process Precision Machinery, China). The galvanized steel substrates ($40 \times 130 \times 1$ mm^3) were rubbed with fine sandpaper to remove galvanized layer and were also scrubbed with acetone several times. The as-prepared coatings

Figure 1. The measuring equipment of the composites in volume resistivity.

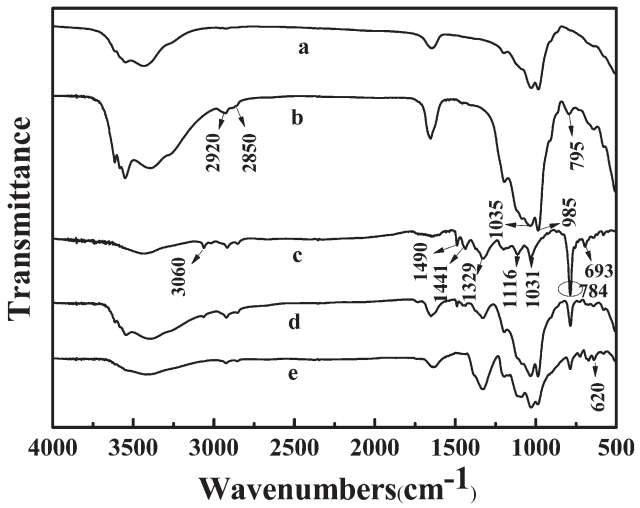

Figure 2. FTIR spectra of PA (a), MPA (b), PTh (c), MPA-PTh (d), and PMPA-PTh (e) composites.

were painted on the surface of the steels in uniformity to prevent overflow phenomenon and the coating thickness was 80–150 μm. The coating films were placed in a cabinet for 24 h at room temperature, and then they were dried 2 h at 70°C.

Materials Characterization

Fourier transform infrared spectra (FTIR) was recorded by using a Nicolet Corporation 460 from 4000–500 cm^{-1}. X-ray photoelectron spectroscopy (XPS) measurement was carried out by VG Corporation (UK) ESCALAB MKII with an Al Kα X-ray source. X-ray diffractograms were performed on Rigaku Corporation (Japan) D/Max 2500 PC X-ray diffraction (XRD) with Cu-Kα radiation of the X-ray wavelength 0.15418 nm over a 2θ range from 5 to 80°. The morphologies for prepared samples were observed by JEOL Corporation (Japan) JEM-2100 transmission electron microscope (TEM) and JSM-6300 scanning electron microscope (SEM), respectively. The specific surface area and pore distribution of the composites were determined by Micromeritics Corporation ASAP2010C surface area and porosimetry system. The electrochemical impedance spectrum (EIS) was measured on a CHI 660D electrochemical analyzer (CH Instruments, Chenhua,

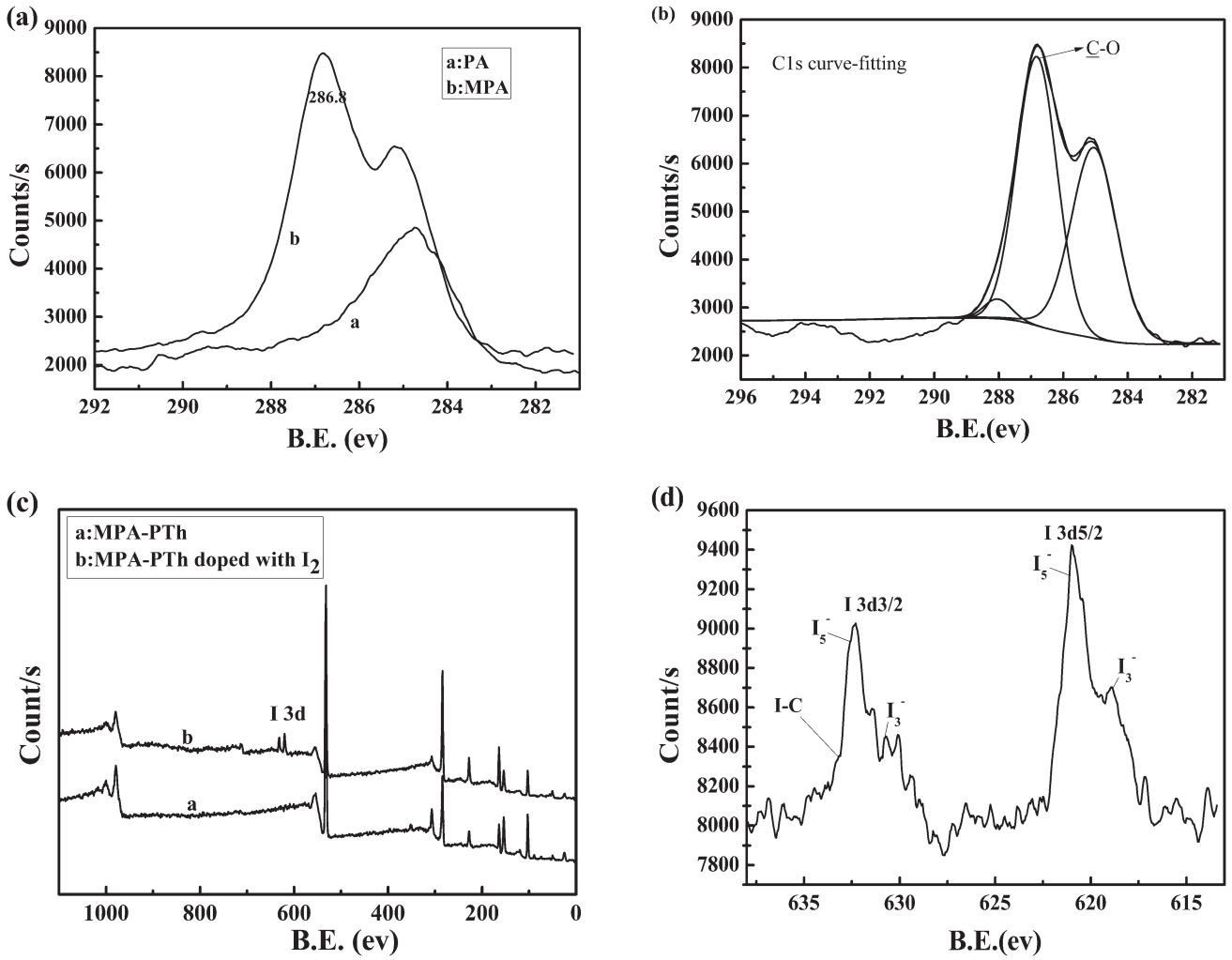

Figure 3. (a) C 1 s scan spectra curve of PA and MPA, (b) C 1 s curve-fitting of MPA, (c) XPS survey full scan spectra of prepared composites, and (d) High resolved iodide XPS spectra.

Applied Polymer SCIENCE

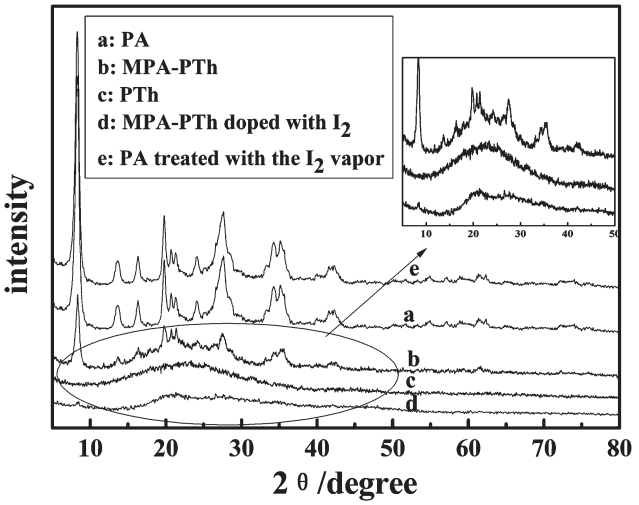

Figure 4. XRD patterns for PA, PTh, and prepared composites.

Shanghai, China). The working electrode was dipped into a mixture solution of 5 mmol L^{-1} $K_3Fe(CN)_6$ and 0.1 mol L^{-1} KCl. The initial voltage was 0.1 V, the ac amplitude was 5 mV and the frequency ranged from 100 kHz to 0.01 Hz.

The volume resistivity of the prepared composites was measured in an efficient and particular self-made equipment: the sample was packed into the copper device in Figure 1 and thus was compressed with 5.0 MPa pressure. The volume resistivity was calculated according to eq. (1):

$$R_{sp} = R \times A/L \quad (1)$$

where R_{sp} is the volume resistivity, R is the measured resistance, A is inner sectional area, L is the length of the sample.

The measurement for the surface resistivity of coating films was performed on YFT-2006 model coating resistivity instrument (Guangzhou Zihui instrument technology, China) and the computational method was in accordance with the Ref. 18.

RESULTS AND DISCUSSION

FTIR Analysis

Figure 2 shows FTIR spectrum of PA, MPA, PTh, and the composites. For MPA, the obvious peak at ~795 cm^{-1} belongs to Si—O—Si bending mode,[19] which is believed to be caused by condensation between the Si—OH of hydrolyzed KH-560 and the one of PA surface. Furthermore, the peaks at ~2920 and ~2850 cm^{-1}, originated from C—H stretching vibration, increase noticeably.

As can also be seen that the spectral data of the prepared PTh is consistent with those reported previously.[5,20] The sharp peak at 784 cm^{-1} can be assigned to C—H out-of-plane stretching vibration, revealing the α-position linkage between the thiophene rings.[21] For the iodine-doped MPA-PTh, the new peak at 620 cm^{-1} could be observed, which is attributed to the monomer specific C—I^- bands.[22] The intensity of Si—OH peak at ~985 cm^{-1} decreases while that of Si—O—Si peak at ~1035 cm^{-1} increases, which might be due to the fact that the PA crystal structure of MPA-PTh has been changed after doped with iodine vapor.

XPS Analysis

Figure 3 shows XPS spectra of PA, MPA, and the composites. For MPA, a new peak of C 1 s at a BE of 286.8 eV becomes remarkably visible in Figure 3(a,b), which is considered as the C—O groups of KH-560.[23] The evidences of FTIR and XPS indicate that KH-560 has been bound to the PA surface. The new peaks of I 3d can be observed in Figure 3(c) and the two characteristic peaks for iodide at 632.3 and 620.9 eV belong to the electronic states of I $3d_{3/2}$ and I $3d_{5/2}$, respectively, in Figure 3(d), implying the existence of iodide in two different states: the main peak can be attributed to I^-_5 and the side peak is ascribed to I^-_3, similar to the argument that is proposed by

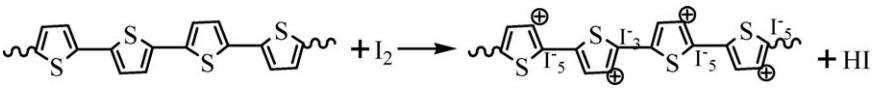

Scheme 2. The formation mechanism of HI acid.

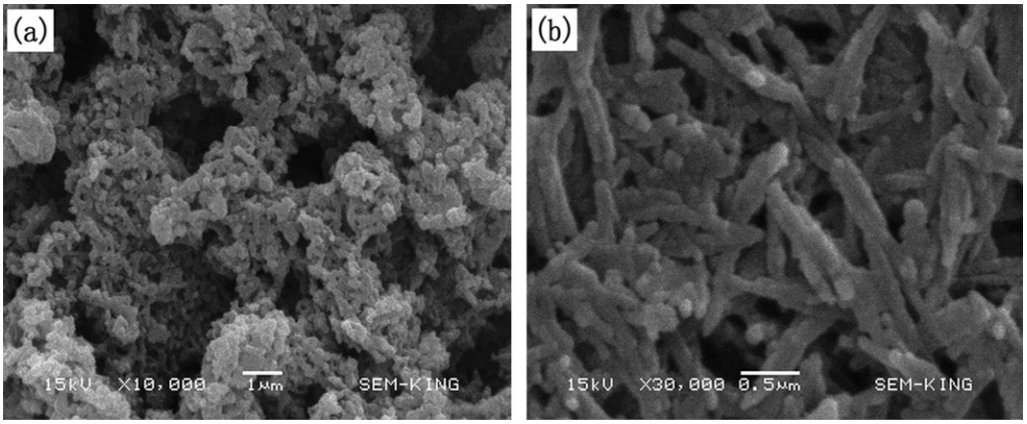

Figure 5. SEM images of PTh (a) and MPA-PTh (b) composites.

Wochnoeski.[22] In addition, the slight C—I$^-$ bonds can be detected, which is largely consistent with FTIR analysis. FTIR and XPS, the formation mechanism of HI acid is shown as Scheme 2.

XRD Analysis

To further confirm the structure of the composites, the XRD patterns are shown in Figure 4. Only one broad peak can be found at the Bragg angle of approximately 24° for amorphous PTh in Figure 4(c), which is in agreement with the Ref. 24. Compared with Figure 4(a), the PA characteristic peak at the Bragg angle of 8.6° remains hardly change but the intensity decreases sharply in Figure 4(b), which is attributed to corrosion from the reaction process[5]; and the original crystal structure of PA is not destroyed completely. Moreover, the PA characteristic peak, remaining constant in Figure 4(e), further decreases and almost disappears in Figure 4(d), we think that the PA has been caught in corrosion from HI acid. Combine

Microstructure Characterization

The morphologies of PTh, PA, and the prepared composites are shown in Figure 5. As can be seen that PTh particles, synthesized without PA, are aggregated to form loose clusters and granular structure with tiny pores [Figures 5 and 6(a)]. However, the MPA-PTh presents a core–shell structure by PTh-coated PA nanorods. Because of the fact that the PA single crystals are disorder, the prepared composites take a state of irregularity and the mesopore space of MPA is filled with PTh in Figure 5(c). Obviously, a crowd of tiny pores like bright stars can be found in Figure 5(e,f), which proved the porosity of MPA-PTh after doped with iodine vapor.

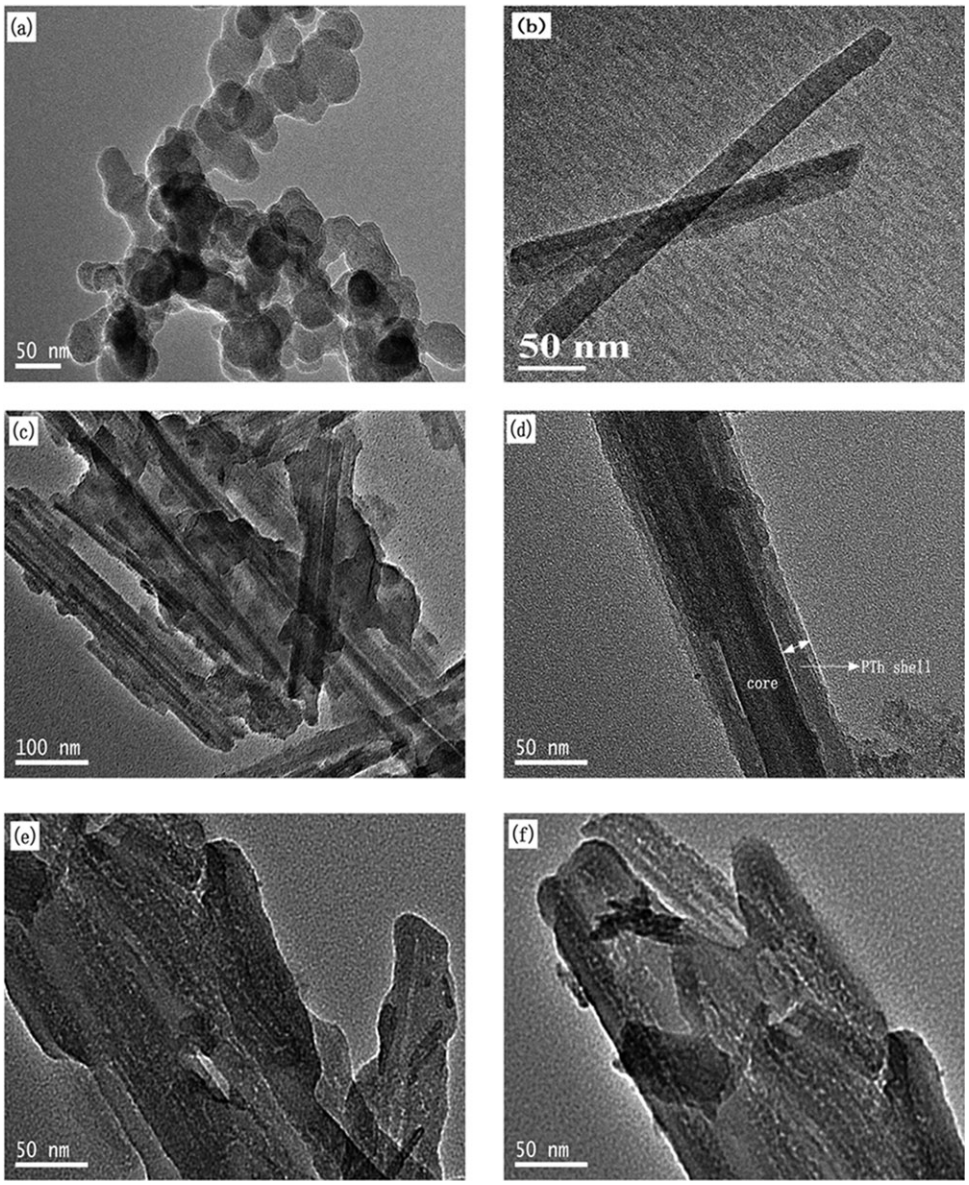

Figure 6. Representative TEM photographs of PTh (a), PA (b), MPA-PTh (c and d), and PMPA-PTh (e and f) composites.

N_2 Adsorption–Desorption Isotherms and Pore Distribution

N_2 adsorption–desorption isotherms and pore distribution of prepared composites at 77.3 K are shown in Figure 7. Obviously, the N_2 volume adsorbed of PMPA-PTh is much larger than that of MPA-PTh at $P/P_0 = 0.98$, which is attributed to the porosity of PMPA-PTh. In addition, the pore distribution of PMPA-PTh becomes wider, and the peak intensity of micropore and mesopore increases noticeably compared with those of MPA-PTh, further supporting that the PA has been transformed into PMPA. Table I summarizes the comparative properties of PTh, MPA-PTh, and PMPA-PTh. It is noticed that the conductivity of PMPA-PTh is superior to that of

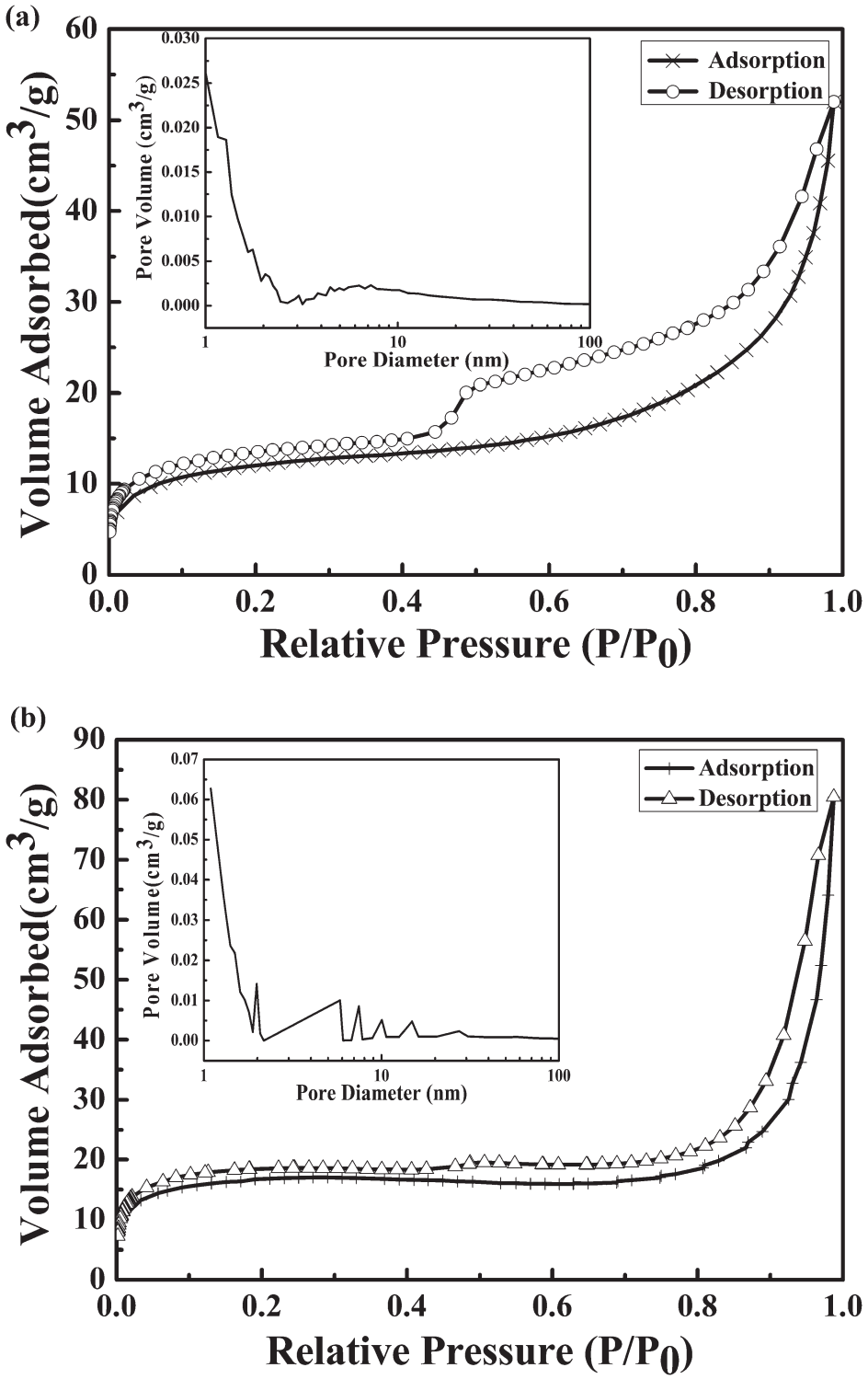

Figure 7. N_2 adsorption–desorption isotherms and pore size distribution of MPA-PTh (a) and PMPA-PTh (b) composites.

Table I. Properties of PTh, MPA-PTh, and PMPA-PTh Composites

Composites	Volume resistivity (Ω·cm)	BET surface area (m^2/g)	BJH average pore size(nm)	BJH cumulative volume of pores (cm^3/g)
I_2-doped PTh	1.53×10^2	-	-	-
MPA-PTh	4.89×10^6	39.57	3.95	0.08
PMPA-PTh	2.44×10^2	52.17	4.28	0.13

MPA-PTh, proving that iodine ion can enter the polymer chains and will more efficiently enhance carrier concentration.[25,26] Similarly, the BET surface area, BJH average pore size and BJH cumulative volume of pores increase correspondingly. Beyond that, the conductivity of MPA-PTh shows little change compared with that of PTh, indicating that the PA was completely encapsulated to form core–shell structure. All of these results are in good agreement with those of FTIR, XRD, and TEM analysis, which demonstrate the fact that the doped MPA-PTh has become the PMPA-PTh conductive composites.

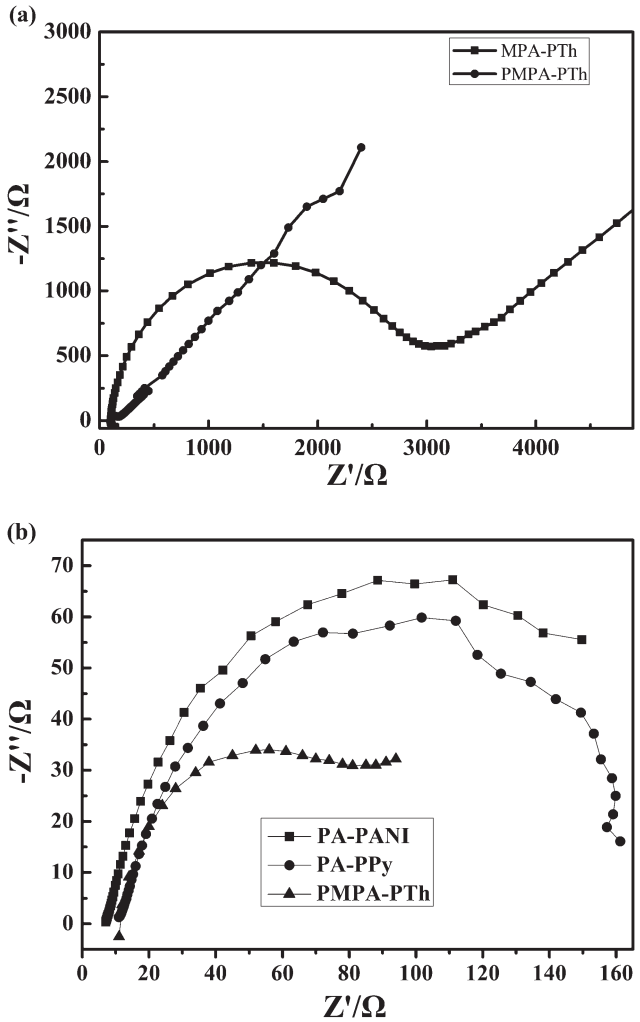

Figure 8. The electrochemical impedances of MPA-PTh and PMPA-PTh (a) and Nyquist plots of PMPA-PTh, PA-PANI, and PA-PPy composites electrodes (b).

EIS Characterization

Figure 8 exhibits the electrochemical impedances of MPA-PTh and PMPA-PTh composites. For Nyquist plots, the shape of semicircle in the high frequency domain expresses the high interfacial charge-transfer resistance, which is assigned to the conductivity of the composites. The sloped portion in the low frequency region is indicative of the Warburg resistance resulting from the frequency dependence of ion diffusion/transport in the electrolyte, suggesting great variations in ion diffusion path lengths and increased obstruction of ion movement.[27,28] It is clear from Figure 8(a) that the internal resistance decreases from ~3000 Ω for MPA-PTh to ~100 Ω for PMPA-PTh, and the Warburg impedance of PMPA-PTh declines compared with that of MPA-PTh, which is recognized as the iodine-doped function. The change is in agreement with that of Table I. As shown in Figure 8(b), of all the composites including PA-PANI, PA-PPy, and PMPA-PTh, the PMPA-PTh shows minimum internal resistance, reflecting its superior conductivity.

Surface Resistivity of the Coating Films

The surface resistivity of composite coating films is discussed in Figure 9. It is seen that the surface resistivity of composite coating films decreases with the increasing content (weight percent). In general, the conductive filler content reaches a certain value (called seepage critical value), the current flows through the charge carrier channel. As a consequence of that, the surface resistivity of composite coatings declines rapidly due to mutual touch. It is noteworthy that the amount of PMPA-PTh is far smaller than that of PTh to get the same surface resistivity,

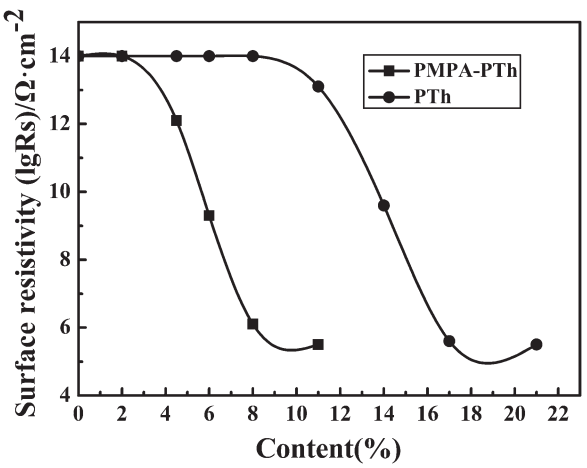

Figure 9. Effect of fillers content on the surface resistivity of coating films.

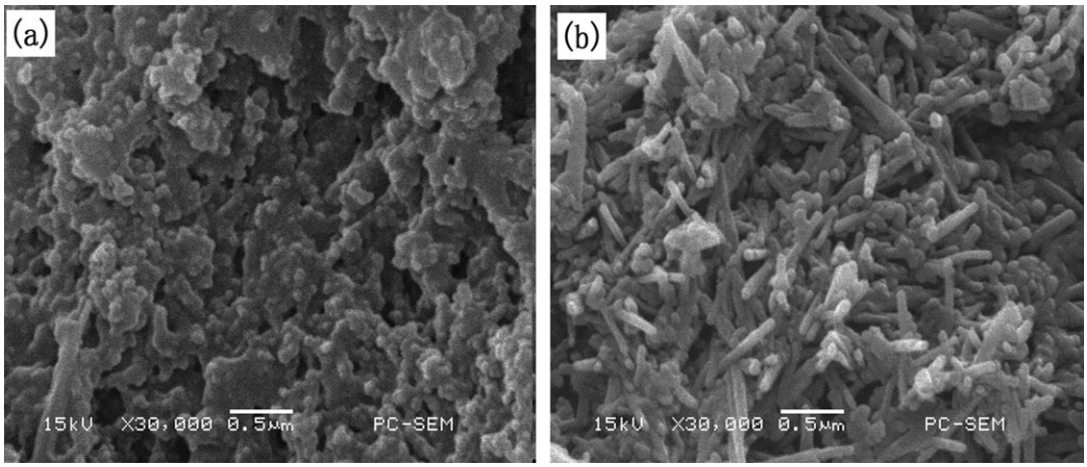

Figure 10. SEM images of composite acrylic conductive coatings of PTh (a) and PMPA-PTh (b).

which is attributed to the formation of the charge carrier channel and the consecutive space network of PMPA-PTh. This can be well explained in Figure 10.

SEM Images of the Coating Films

Figure 10 shows that the SEM images of composite acrylic conductive coatings in the condition of 8% filler. The PMPA-PTh nanorods observed in acrylic coatings take an interlaced state to produce the conductive tunnel.[29] It is easier to touch each other to form conductive network for the PMPA-PTh nanorods than for the PTh particles, which makes PMPA-PTh composite acrylic coating films have the advisable conductivity.

CONCLUSIONS

In this article, the PMPA-PTh conductive composites were obtained successfully. The results showed that the gas phase doping of iodine could transform the MPA-PTh into the PMPA-PTh and improve the electrical conductivity of composites simultaneously. The volume resistivity, the internal resistances and the Warburg resistance of the PMPA-PTh were enhanced significantly compared with those of the MPA-PTh, as well as the BET surface area, the BJH average pore size and the BJH cumulative pore volume. The PMPA-PTh composites could form consecutive network frame and could improve the conductivity of acrylic coatings.

ACKNOWLEDGMENTS

This work was supported by the Natural Science Foundation of China (51002016), Technology Innovation Team of Colleges and Universities Funded Project of Jiangsu Province (2011-24), the Priority Academic Program Development of Jiangsu Higher Education Institutions (PAPD), Research and Innovation Plan Project for College Graduates of Jiangsu Province (CXZZ12_0185), Technology Support Plan of Jiangsu Province (BE2011125), Technology Support Program of Changzhou City (CE20110017) and the State Key Program of the Natural Science Foundation of Jiangsu Province (BK2011024). The authors thank the reviewers for critical comments to improve on this work.

REFERENCES

1. Yang, C.; Liu, P.; Wang, T. M. *ACS Appl. Mater. Interfaces* **2011**, *3*, 1109.
2. Yang, X. G.; Li, B.; Wang, H. Z. *Prog. Org. Coat.* **2010**, *69*, 267.
3. Wu, F.; Chen, J. Z.; Chen, R. J.; Wu, S. X.; Li, L.; Chen, S.; Zhao, T. *J. Phys. Chem. C* **2011**, *115*, 6057.
4. Wang, Z. M.; Liu, E. J.; Zhao, X. *Thin Solid Films* **2011**, *519*, 5285.
5. Li, X. G.; Li, J.; Meng, Q. K.; Huang, M. R. *J. Phys. Chem. B* **2009**, *113*, 9718.
6. Uygun, A.; Turkoglu, O.; Sen, S.; Ersoy, E.; Yavuz, A. G.; Batir, G. G. *Curr. Appl. Phys.* **2009**, *9*, 866.
7. Ai, X.; Anderson, N.; Guo, J. C.; Kowalik, J.; Tolbert, L. M.; Lian, T. Q. *J. Phys. Chem. B* **2006**, *110*, 25496.
8. Vu, Q. T.; Pavlik, M.; Hebestreit, N.; Pfleger, J.; Rammelt, U.; Plieth, W. *Electrochim. Acta* **2005**, *51*, 1117.
9. Uygun, A.; Yavuz, A. G.; Sen, S.; Omastova, M. *Synth. Met.* **2009**, *159*, 2022.
10. Yang, H. M.; Tang, A. D.; Ouyang, J.; Li, M.; Mann, S. *J. Phys. Chem. B* **2010**, *114*, 2390.
11. Xu, J. X.; Zhang, J. P.; Wang, Q.; Wang, A. Q. *Appl. Clay Sci.* **2011**, *54*, 118.
12. Song, L.; Fang, S. L.; Zhan, J.; Hu, Y.; Wu, J. *Polym. Compos.* **2010**, *31*, 405.
13. Wang, L. H.; Sheng, J. *Polymer* **2005**, *46*, 6243.
14. Shen, S. G.; Yang, M.; Ran, S. L.; Xu, F.; Wang, Z. X. *J. Polym. Res.* **2006**, *13*, 469.
15. Liu, Y. S.; Liu, P.; Su, Z. X. *Synth. Met.* **2007**, *157*, 585.
16. Yang, C.; Liu, P. *Synth. Met.* **2009**, *159*, 2056.
17. Yao, C.; Xu, Y. Y.; Kong. Y.; Liu W. J.; Wang, W. J.; Wang, Z. L.; Wang, Y.; Ji, J. L. *Appl. Clay Sci.* **2012**, *67–68*, 32.
18. Li, J.; Qian, X. R.; Chen, J. H.; Ding, C. Y.; An, X. H. *Carbohydr. Polym.* **2010**, *82*, 504.
19. Kim, M. T. *Thin Solid Films* **1997**, *311*, 157.
20. Li, X. G.; Li, J.; Huang, M. R.; *Chem. Eur. J.* **2009**, *15*, 6446.

21. Lu, M. D.; Yang, S. *Synth. Met.* **2005**, *154*, 73.
22. Wochnoeski, C.; Metev, S. *Appl. Surf. Sci.* **2002**, *186*, 34.
23. Chen, Y.; Zhao, Y. J.; Zhou, S. Y.; Chu, X. Z.; Yang, L. L.; Xing. W. H. *Appl. Clay Sci.* **2009**, *46*, 148.
24. Kong, F. H.; Wang, Y.; Zhang, J.; Xia, H. J.; Zhu, B. L.; Wang, Y. M.; Wang, S. R.; Wu, S. H. *Mater. Sci. Eng. B* **2008**, *150*, 6.
25. Noma, N.; Kawaguchi, K.; Imae, I.; Shirota, Y. *Synth. Met.* **1997**, *84*, 597.
26. Kitao, S.; Matsuyama, T.; Seto, M.; Maeda, Y.; Masubuchi, S.; Kazama, S. *Synth. Met.* **1995**, *69*, 371.
27. Ryu, K. S.; Lee, Y.; Han, K. S.; Kim, M. G. *Mater. Chem. Phys.* **2004**, *84*, 380.
28. Zhang, K.; Zhang, L. L.; Zhao, X. S.; Wu, J. S. *Chem. Mater.* **2010**, *22*, 1392.
29. Shao, L. A.; Qiu, J. H.; Liu. M. Z. *Chem. Eng. J.* **2010**, *161*, 301.